Motor Cortical Activity During Drawing Movements: Population Representation During Spiral Tracing

DANIEL W. MORAN AND ANDREW B. SCHWARTZ
The Neurosciences Institute, San Diego, California 92121

Moran, Daniel W. and Andrew B. Schwartz. Motor cortical activity during drawing movements: population representation during spiral tracing. *J. Neurophysiol.* 82: 2693–2704, 1999. Monkeys traced spirals on a planar surface as unitary activity was recorded from either premotor or primary motor cortex. Using the population vector algorithm, the hand's trajectory could be accurately visualized with the cortical activity throughout the task. The time interval between this prediction and the corresponding movement varied linearly with the instantaneous radius of curvature; the prediction interval was longer when the path of the finger was more curved (smaller radius). The intervals in the premotor cortex fell into two groups, whereas those in the primary motor cortex formed a single group. This suggests that the change in prediction interval is a property of a single population in primary motor cortex, with the possibility that this outcome is due to the different properties generated by the simultaneous action of separate subpopulations in premotor cortex. Electromyographic (EMG) activity and joint kinematics were also measured in this task. These parameters varied harmonically throughout the task with many of the same characteristics as those of single cortical cells. Neither the lags between joint-angular velocities and hand velocity nor the lags between EMG and hand velocity could explain the changes in prediction interval between cortical activity and hand velocity. The simple spatial and temporal relationship between cortical activity and finger trajectory suggests that the figural aspects of this task are major components of cortical activity.

INTRODUCTION

Recently, studies of multijoint arm movement have shown that a set of spike trains recorded from motor cortex can be used to predict the direction and speed of movement (Moran and Schwartz 1999; Schwartz 1992). In fact, the arm's trajectory is well represented in this activity when considered as a population during reaching (Georgopoulos et al. 1988; Moran and Schwartz 1999) and drawing (Schwartz 1993; Schwartz and Moran 1999), suggesting that this technique can provide a detailed prediction of the behavior to take place in the immediate future. Drawing is characterized by a linkage between the kinematics of the movement and the shape of the figure to be drawn. In general, as the curvature of a figure increases, the speed of the hand decreases. Specifically, angular velocity is proportional to curvature raised to the ⅔ power; a relation known as the "⅔ power law" (Lacquaniti et al. 1983), or, alternatively, that speed is proportional to curvature to the $-⅓$ power. We examined spiral drawing because the radius of curvature (ρ) changes linearly with the extent or arc length of the figure. With the aim of elucidating the predictive behavior of the cortical-movement system, we used this linear relation to examine the timing of the directional signal as it changed within the task. To measure the temporal characteristics of this process we calculated a "prediction interval" (PI) as the time interval between the cortical representation of a direction and the occurrence of that direction in the movement. This interval increased throughout the spiral as it was drawn from outside→in and decreased when drawn inside→out. Curvature ($1/\rho$) increases or decreases depending on the direction of drawing and the PI changed consistently when plotted against curvature for spirals drawn in either direction, suggesting that curvature is the primary determinant of the prediction interval.

The ability to use population activity to visualize accurately the shape of the figure to be drawn suggests a movement plan in motor cortex. By examining the timing between the directions specified in this plan and their appearance in the movement, it is possible to infer some of the dynamic principles used in the control of this type of arm movement. A short report of these results has been published (Schwartz 1994).

The costs of publication of this article were defrayed in part by the payment of page charges. The article must therefore be hereby marked "*advertisement*" in accordance with 18 U.S.C. Section 1734 solely to indicate this fact.

METHODS

The behavioral paradigm, surgical procedures, and general animal care were approved by the Institutional Animal Care and Use Committee. The outlines put forth by the Association for the Assessment and Accreditation of Laboratory Animal Care and the Society for Neuroscience were followed.

Behavioral task

Monkeys were trained using operant conditioning to draw various figures with a single finger on a touchscreen (Moran and Schwartz 1999). Each monkey performed a sequence of tasks after each cell was isolated. A center→out task was followed sequentially by sinusoidal, spiral, and figure-eight drawing tasks. Drawing tasks began with a circle (10–11 mm radius) displayed on the screen to indicate the starting location of the task. The animal placed and held its finger in this circle for 100–300 ms (hold period). At the end of this interval, the entire figure to be traced was displayed, and the animated circle was moved a small increment along the figure away from the animal's finger. The animal was required to keep its finger on the screen surface and move to the newly displaced circle. As soon as the finger touched the target circle, the circle moved again, following the outline of the spiral. Repeating this process resulted in an animated sequence with the circle continuously just ahead of the smoothly moving finger. The surface of the touchscreen was lubricated daily with mineral oil to minimize friction with the sliding finger of the monkey. If the animal lifted its finger from the screen or did not move its finger to the newly displaced target circle within a 300 ms increment, the trial was aborted. The rate of the movement was determined by the animal because the constrained time increment was generous enough to allow

very slow movements. After several weeks of training, smooth continuous movements were made with this approach. Spirals were presented as two classes in five randomized blocks. In the first class, the spiral was traced from outside→in; in the second class, it was traced from inside→out. Each spiral consisted of three circuits: the outer radius was 7.5 cm, and the innermost radius was 1.5 cm. A liquid reward was administered at the end of a successful trial (a complete tracing of the figure). This sequence of tasks was repeated with each isolated cell.

Cortical and electromyographic recording (EMG) technique

Glass-coated platinum-iridium electrodes were used to record single motor cortical units extracellularly. Both intramuscular or epimysial electrodes were used to record electromyographic data from various shoulder/elbow muscles. These techniques are described in the preceding paper (Moran and Schwartz 1999).

Kinematic recording technique

With the use of three-dimensional (3-D) positional data recorded from various points on the arm during a trial, shoulder and elbow joint angles were calculated as a function of time. The monkey's arm was fitted with a lightweight hinged orthosis that was strapped to both the upper and lower arm with the hinge centered over the elbow joint. Three infrared emitters were attached to the orthosis: one on each end of the device (wrist and shoulder marker) and the third close to the hinge on the forearm segment. An Optotrak 3010 motion analysis system (Northern Digital, Waterloo, Ontario) sampled the 3-D position of the three markers at 100 Hz during the drawing tasks. The movement data were digitally filtered using a phase-symmetrical, natural B-spline (quintic order) with a low-pass cutoff frequency of 10 Hz (Woltring 1986). The distance between the center marker and the hinge (elbow) was measured with a caliper at the beginning of each experiment.

To generate joint angles, attitude matrices were calculated for both the upper and lower arm segments. With the use of the distance from the center marker to the elbow and the vector connecting the center marker to the wrist marker, the 3-D location of the elbow joint was calculated. The vectors from the wrist marker to the elbow joint and the elbow joint to the shoulder marker defined the long axes (y) of the two segments. Assuming a single degree of freedom (DOF) for the elbow joint, the medial/lateral (z) axes for each segment are equal and were calculated by a vector cross product of the two long (y) axes vectors. Finally, the posterior/anterior (x) axes of the segments were calculated from vector cross products of their z- and y-axes. The axes vectors were normalized to generate 3×3 attitude matrices for both the forearm and upper arm. The torso of the monkey was assumed fixed and aligned with the global reference frame such that its attitude matrix equaled the identity matrix. Rotation matrices for both the shoulder and elbow joint were generated from the segmental attitude matrices. Finally, Cardanic angles (Euler permutation x, y', z'') were calculated from the direction cosines of the rotation matrices resulting in three shoulder joint angles (adduction[+]/abduction[−], internal[+]/external[−] rotation and flexion[+]/extension[−]) and a single elbow angle (flexion[+]/extension[−]). The anatomic position (i.e., hands hanging down at sides) represented the posture in which all joint angles were zero.

Single-cell analysis

Each trial for a particular class was divided into 100 bins over the movement time. In addition, 10 "prebins" were calculated for the period just before movement onset. Every prebin had the same time width as a movement bin, and fractional intervals (Richmond et al. 1987; Schwartz 1993) were calculated throughout all 110 bins. These values were averaged across trials within classes, binwise. The resulting average firing rates were low-pass filtered (ccsmh, IMSL, Visual Numerics, Houston, TX) and square-root transformed (Moran and Schwartz 1999). Average trajectories were calculated using the finger displacement data that had been collected simultaneously. Using the same low-pass filter function (ccsmh, IMSL), the x and y finger coordinates were temporally normalized to 101 instants encompassing the 100 movement bins. For each trial and in every bin, the velocity of the finger was calculated. These velocities were either averaged across the five trials recorded in a single experiment or across all experiments for comparison to population vectors.

To test the directional sensitivity of these individual cell responses across time within a single task, it was necessary to transform movement directions into firing rates. We used the instantaneous direction of the movement in each bin of the spiral task and the tuning parameters of the cell derived from the center→out task (*Eq. 3* of the previous paper, Moran and Schwartz 1999) to generate a simulated discharge rate in each bin of the drawing task (Schwartz 1992). The resulting time series of simulated discharge rates for an entire trial was compared with the actual discharge rates of that cell using cross-correlation. The time lag of the peak-positive correlation was used as an indication of the average interval (AI) between a direction predicted by a single cell's activity and the movement of the finger in that direction. This not only tested the directional sensitivity of the neuron within the task but also showed whether the tuning function was robust and valid across different types of tasks.

Population vector analysis

The method used to construct population vectors has been described in detail in previous papers (Moran and Schwartz 1999; Schwartz 1993). Population vectors were calculated in each of the 110 bins for both classes. The preferred direction of each cell included in the study was calculated from the center→out task; the assumption is made that the cell's preferred direction is constant between different tasks (center→out, spiral, *etc.*) and within a given movement. Both the movement vectors and population vectors were converted from a cartesian coordinate system (x, y) to a polar system (θ, r) where direction and magnitude were independently smoothed using a cubic spline function ("ccsmh," IMSL). "Neural trajectories" were generated by integrating the time series of population vectors (Moran and Schwartz 1999) as a movement path representation in the cortical activity.

To investigate the time relation between the isomorphic representation of the spiral shape present in the cortical population activity and the movement of the hand along that path, it was necessary to match individual population directions to movement directions. Because spiral drawing essentially consists of contiguous circular movements, the directional component (θ) of movement velocity is a monotonic function of time; it increases continually for outside→in (counterclockwise) movements and decreases for inside→out (clockwise) movements. When direction crossed the 2π-0 radian transition, 2π was added to the remaining directions to eliminate discontinuities in the directional profile; the reverse was done for clockwise movements. The directional components of both neural population and movement velocity vectors were fit with a third-order polynomial ("rcurv," IMSL) to assure that direction changed monotonically. The population vector directions were applied as abscissa data (time being the ordinate) to a cubic spline routine ("csakm," IMSL). (Note: spline routines require that abscissa data (knots of the spline) be either steadily increasing or decreasing (i.e., monotonic) so that the ordinate data are a function of the abscissa data. The validity of these operations can be assessed by comparing the processed directions to the raw unsmoothed directions presented in RESULTS. The movement direction data were fitted with the same spline routine but in the reverse order of the population data (i.e., time was the abscissa, and direction was the ordinate). For any instant of movement time, the corresponding movement direction could then be interpolated from the movement

spline. This direction was then applied to the spline of population vector directions, and its corresponding interpolated time was subtracted from the movement time instant. We refer to this time interval as the "prediction interval" (PI). This differs from the average interval derived from the cross-correlation of simulated and actual discharge rates of individual cells described above. There is only one AI for each trial in contrast to a continuum of values for the PI. The PI is a descriptor of the timing between population vector direction and movement velocity direction; the AI refers to the average lag between simulated and actual discharge rates in an individual cell.

RESULTS

The activity patterns of 318 cells from 4 hemispheres of 2 monkeys were included in this study. The recordings sites as determined by the location of electrode penetrations were shown in the previous paper (Moran and Schwartz 1999). Of these cells, 77 were recorded in the same dorsal premotor area. The remainder were in the primary motor cortex. Cells were included in this study if they were directionally tuned ($r > 0.84$ for the cosine fit in the center→out task), fired during the task, and were passively driven by movements of the shoulder and/or elbow joints. The cells included in this study are a subset of those analyzed in the previous reaching paper (Moran and Schwartz 1999). Initially we will consider the results of the primary motor cortical cells (3 hemispheres). Later we will compare the behavior of premotor to primary motor cortical cells in a single animal.

The animals were well trained before data collection began. The top of Fig. 1 shows the trajectories averaged over all the recorded trials for both directions of tracing. The largest radius of the trajectories was 7.7 cm, and the smallest, in the center of the spiral, was 1.2 cm. An example tracing obtained for a single motor cortical cell can be seen in the bottom of Fig. 1, whereas the rest of the data recorded for the example are shown in Fig. 2. The top row of the figure shows spike activity raster plots for the outside→in and inside→out spiral. The corresponding histograms in the second row exemplify the harmonic firing rates typically seen during this task. As expected, this activity is well correlated with the cosine of movement direction (3rd row). In contrast, the movement speed (4th row) is not well modulated in this task. There is, however, a tendency for the hand to slow in the more curved part of the figure. As the monkey's finger slows down in the inner, highly curved portion of the spiral, the peak amplitudes of cortical modulation also declined. Shoulder and elbow joint angles (rows 5–8) are also harmonic, showing that intrinsic kinematic variables covary with extrinsic finger direction and, hence, cortical activity. Finally, the last five rows of Fig. 2 show that muscle activity is also harmonic. This cell, and indeed many of the cells we studied, had an activity pattern that was correlated with finger direction, joint angles, and muscle activity. Many movement parameters are interrelated during these drawing tasks.

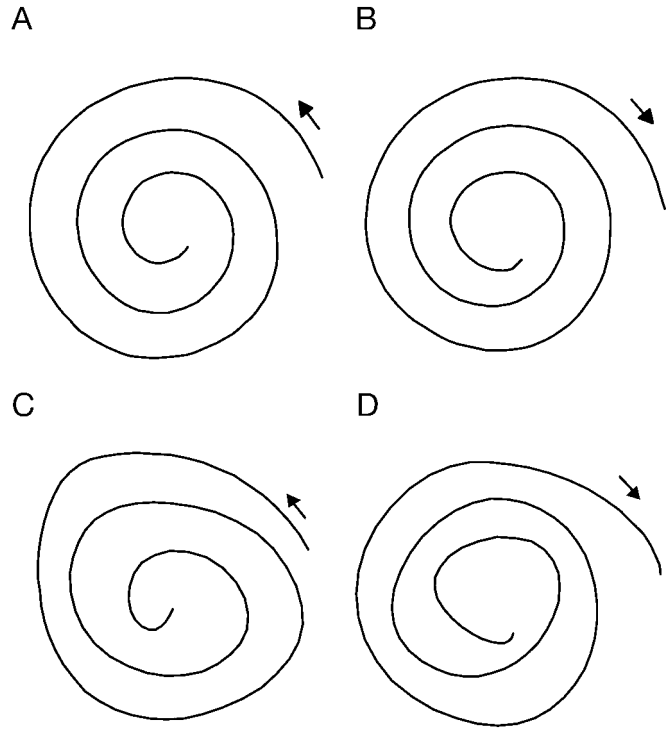

FIG. 1. Average ($n = 1{,}590$) finger trajectories during the 2 classes of spiral drawing. In the 1st class (*A*) the animal traced the figure from outside→in. The same template was traced from inside→out in the 2nd class (*B*). Finger trajectories for a single example cell ($n = 5$) can be seen in *C* and *D*.

Single-cell responses

PRIMARY MOTOR. Trial movement times were divided into 100 bins, and the average discharge rate and movement velocity (direction and speed) were calculated for each bin. On average, the monkeys performed the spiral tasks in 2.5 s, yielding binwidths of ~25 ms (outside→in = 24.3 ± 2.6 ms, mean ± SE; inside→out = 25.2 ± 3.5 ms). In addition, 10 prebins were calculated for the neural activity occurring just before movement onset (~250 ms). Using the center→out tuning equation for each cell, simulated discharge activity was calculated using the movement direction in each bin. Figure 3 compares the simulated and actual discharge activity for an example cell during both classes of spirals. Like the actual activity, the simulated activity is harmonic; as the movement direction crosses the preferred direction, the discharge activity is maximal; when the movement direction is in the anti-preferred direction, the activity is minimal. An important feature in both the outside→in and inside→out spirals is the relative timing between the actual and simulated discharge rates. The time difference between the two profiles can be considered as the interval between the representation of direction in the activity of the cell and the occurrence of that direction in the movement. The average correlation between the actual and predicted discharge rates over the entire movement can be measured with conventional cross-correlation. The two sets of profiles were highly correlated (*A*: $r = 0.79$, *B*: $r = 0.95$) with lags of 77 and 94 ms, respectively. The same comparison was made for each of the primary motor cells (for both classes of drawing). A histogram of their peak correlation coefficients for the 241 primary motor cells in this study is shown in Fig. 4*A*. This distribution is unimodal with a mean of 0.57 ($n = 482$). The time interval that would best align the predicted and actual discharge rates was also calculated for those cells with significant correlations ($p < 0.01$). Over 88% of the cells had significant correlations for both classes of drawing. A histogram of these time lags (for values lying between 350 ms before and 250 ms after the movement) is plotted in Fig. 4*B*. The mean of this distribution ($n = 404$) shows that on average,

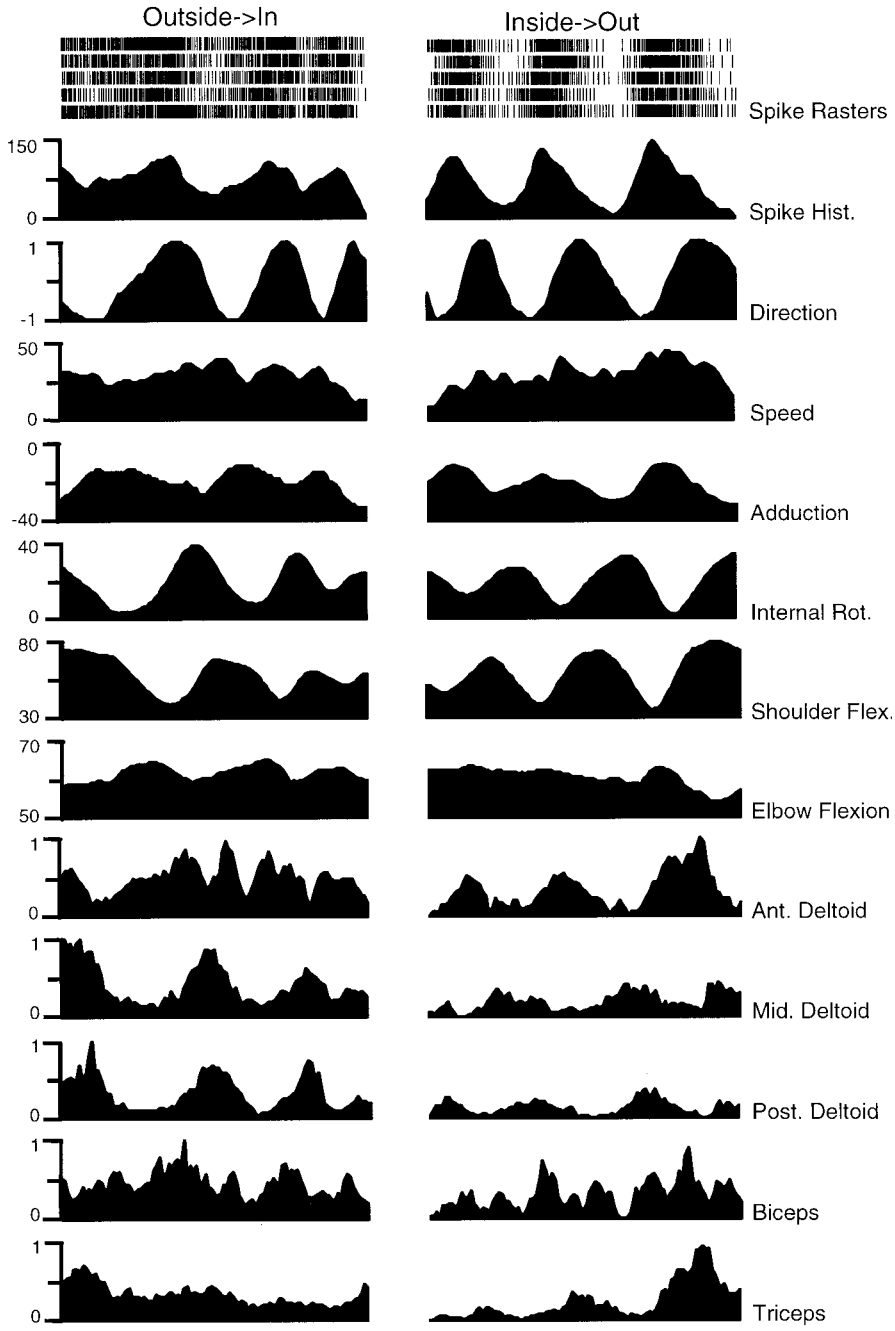

FIG. 2. Typical data set recorded for a single cell. *Top row*: 5-trial rasters for a motor cortical cell during both an outside→in (*left*) and inside→out tracing. *Second row*: histograms were made by converting the raster data into firing rates (spikes/s) and averaging across the 5 trials. The cosine of finger direction (*row 3*), shows a harmonic relation to the neural activity. There is a weak tendency for higher finger speeds (*row 4*) on the outside of the spiral and for slower speeds in the interior of the spiral. Four joint angles (*rows 5–8*) were calculated for the shoulder and elbow joints. Finally, *rows 9–13* show the average muscle activity (electromyographic, EMG) recorded during the trials.

the directional information contained in the discharge activity of these cells predicts the movement of the finger by 90 ms.

COMPARISON OF PRIMARY MOTOR AND PREMOTOR CELL RESPONSES. To compare primary and premotor cortical activity in the same animal, a subset of the total data were used. Correlation analysis was applied to the cortical activity of 77 cells from the left dorsal premotor and 71 cells from the right primary motor cortex of the same animal. Correlation coefficients from the analysis of the predicted and actual discharge rates for each of these cells are shown in Fig. 5*A*. The means are 0.42 ($n = 154$) for the premotor cells and 0.52 ($n = 142$) for the primary motor cortical cells. Only 64% of premotor cell trials showed significant correlations for both classes of spirals, whereas over 86% of the primary motor cell trials were significant. The timing of the two sets of cells is shown by their significant correlation lags in Fig. 5*B*. The average primary motor lag was 80 ms. Interestingly, the premotor cell responses had a bimodal distribution with peaks at 0 and 250 ms.

Population responses

DIRECTION COMPARISON. Population vectors were constructed from the total sample of primary motor cortical cells ($n = 241$) for both movement classes. The 110 bins of each trial were used to create 110 population vectors for each class. Finger displacement data were used to calculate 100 movement velocity vectors. The 110 population and 100 movement vectors for each class are shown in Fig. 6. Visual inspection suggests that the population and movement vectors are very similar for

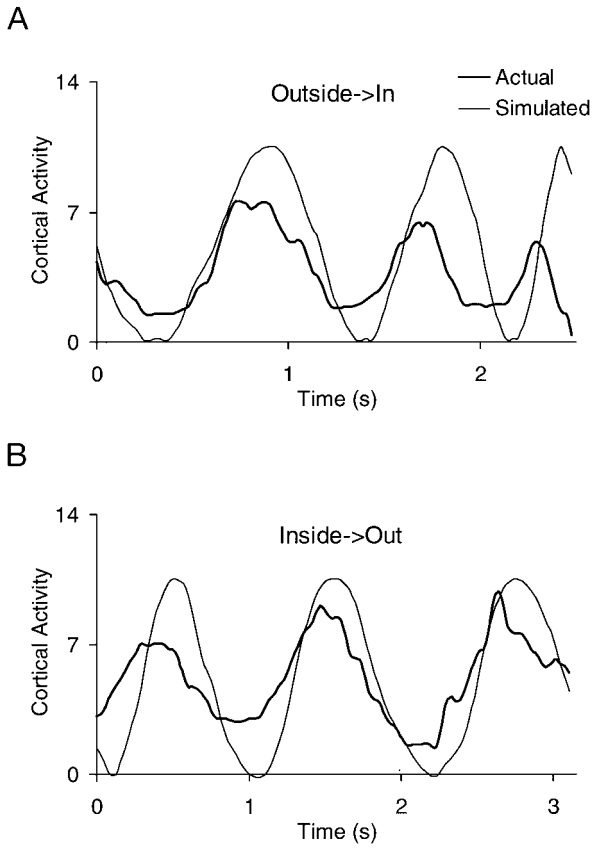

FIG. 3. Simulated and actual discharge rates for an example cell. Tuning information from the center→out task was used to calculate a predicted discharge rate for the cell using finger direction. The neural activity was found to be highly correlated (*A*: $r = 0.79$ at 77 ms; *B*: $r = 0.95$ at 94 ms) to the simulated discharge rates.

each class. Indeed, using vector field analysis (Shadmehr and Mussa-Ivaldi 1994), the correlation between the 100 movement vectors and 100 population vectors yields a coefficient of 0.97 for the outside→in spiral and 0.96 for the inside→out spiral. (Note: the 100 population vectors chosen consisted of the last 4 prebins and the 1st 96 task bins. This corresponds to average shift of 100 ms, which is in agreement with Fig. 4*B*.)

The directions of the population and movement vectors are compared in Fig. 7. Population vector direction is shown as the thick line, whereas the movement direction is the thin line. The unfiltered population vector directions are also included in Fig. 7 (•) to illustrate the raw data. There is a very good match of population vector and movement vector direction as represented by the slope and shape of these curvilinear traces. In the outside→in task, the two directions are coincident initially, and then diverge slightly. The opposite description applies to the inside→out task, where the two directions are disparate initially and then converge toward the end of the task. The instantaneous interval (prediction interval) between the two traces in each class was measured along the horizontal. Because the spirals were drawn outwardly and inwardly, the convergence-divergence of the direction traces is related to the position of the finger on the spiral.

TIMING CHARACTERISTICS. The spirals were constructed so that the radius of curvature changed linearly with position along the figure; the radius of curvature is correlated with position that, in turn, is related to prediction interval. In addition, finger speed is tightly coupled to curvature (Lacquaniti et al. 1983) and is also related to the prediction interval. Both curvature and speed as a function of time are plotted in Fig. 8. In general, curvature and speed are inversely related. The prediction intervals were plotted against curvature, radius of curvature, and speed for both classes (Fig. 9). Although both parameters show a relationship to prediction interval, the curvature-PI relation (Fig. 9, *A* and *B*) appears more consistent ($r = 0.98, 0.98$) than the speed-PI relation (Fig. 9*C*, $r = 0.92$). At small curvatures, the prediction interval is small. When the curvature is 0.18–0.20 cm^{-1}, the prediction interval rises rapidly. The curves approach an asymptote around 0.4 cm^{-1} and thereafter have an approximately constant value of 100 ms. When PI is plotted against the radius of curvature (inverse of curvature), the relation is strikingly linear (O→I, $r = 0.98$; I→O, $r = 0.98$), and the data from both classes overlap. The prediction interval is a direct function of the instantaneous radius of the figure. In the straightest portions of the spiral, the direction signal occurs 40 ms before the movement and when the path is curved, this interval rises to 100 ms.

This finding differs from point-to-point reaching movements which have average intervals of 125–150 ms (Moran and Schwartz 1999). One reason for this difference may be the parameters used to calculate the lags. The lags calculated in the point-to-point reaching data were based on finger speed,

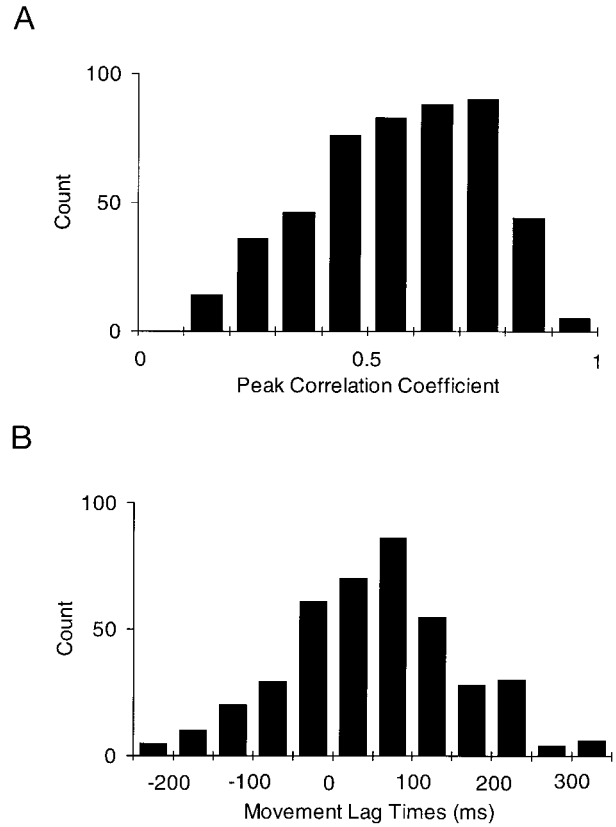

FIG. 4. *A*: histogram of peak correlation coefficients between the actual and predicted firing rates of 241 primary motor cortical cells (3 hemispheres). The drawing task consisted of 2 opposite spiral movements yielding a total histogram count of 482. *B*: histogram of movement lags between actual and predicted firing rates as determined from cross-correlation. Only correlations from *A* that were significant ($p < 0.01$) are shown ($n = 404$). The figure illustrates that the majority of motor cortical cells lead the movement.

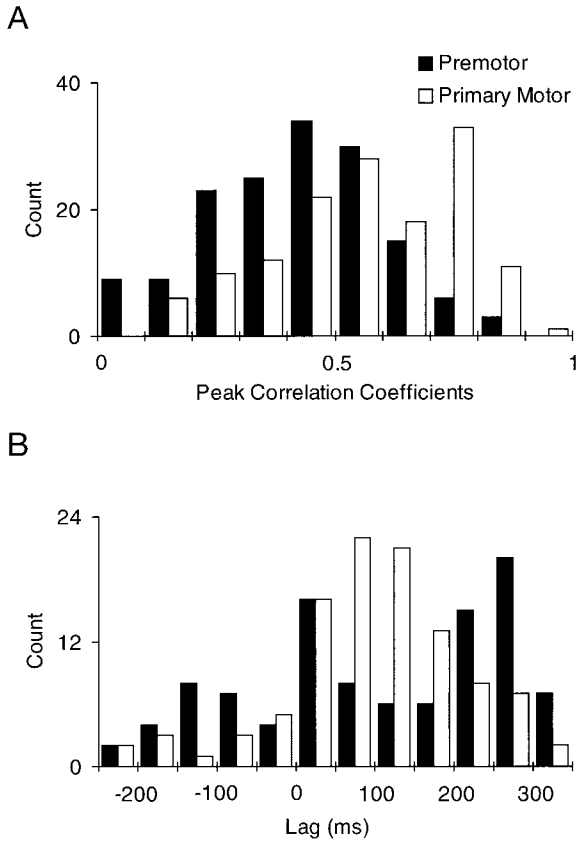

FIG. 5. *A*: comparison of peak correlation coefficients from premotor and primary motor areas in a single monkey. In the motor cortex (right hemisphere), 71 units were recorded. Recordings were made from 77 premotor cortical cells in the contralateral hemisphere. Overall, the firing rates from primary motor cortical cells have higher correlation with predicted rates than premotor cells. *B*: histogram of time lags found from significant premotor correlations ($n = 103$) and a similarly sized population of primary motor ($n = 103$) correlations. As in Fig. 4*B* the primary motor cortical cells have a unimodal distribution with an average lead time of 100 ms. The premotor cortical cells show a bimodal distribution with lead times of 250 and 0 ms.

whereas in this study they are based on finger direction. The time lags pertaining to these two parameters may be independent (Schwartz and Moran 1999). It should also be noted that we are comparing time lags throughout the movement, not just at the beginning. In fact, the neuronal processing associated with movement initiation may differ from those associated with ongoing control. To examine the transient activity responsible for time lags at movement onset, we used data that had not been smoothed. Population vector directions were calculated from 250 ms before through 400 ms after movement onset and compared with velocity vectors that began at movement onset. (Note: the hand was moving at a near-maximal speed as it exited the start circle border at "movement onset".) Lags were calculated from the directions using the same algorithm outlined above, and the result can be seen in Fig. 10.

Both the outside→in and inside→out spirals in Fig. 10 show rapidly decaying lags occurring during movement onset. In the case of the outside→in spiral, the transiently decaying lag lasts 225 ms. The inside→out spiral also has a fast decaying lag at movement onset lasting ~125 ms, which levels off and is followed by a much slower decaying lag. The initial lags (100–150 ms) are comparable with those found in the center→out task. After 250 ms, these transient lags are gone,

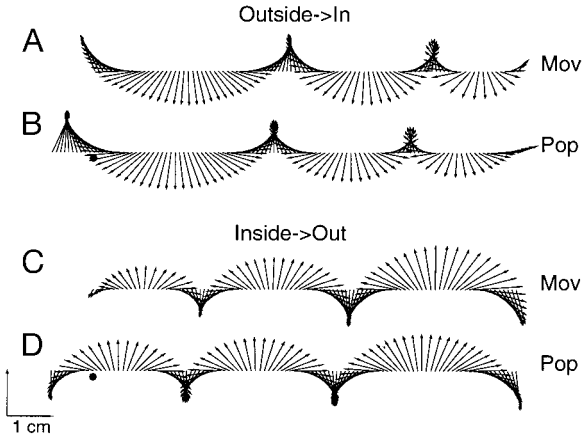

FIG. 6. Vectograms of both movement (*A* and *C*) and population (*B* and *D*) vectors for the 2 classes of spiral movement. The population vectograms were generated using the primary motor cortical cells from all 3 hemispheres ($n = 241$). The population vectograms are composed of 110 vectors, the 1st 10 of which occur before movement onset. Movement vectograms each contain 100 vectors occurring during the movement. On average, each vector accounts for 25 ms of movement time yielding a total movement time of 2.5 s. The 10 "prebins" vectors for the population vectograms represent neural activity occurring 250 ms before movement onset (●).

and the lags follow the pattern apparent in Fig. 7. Figure 10 suggests that there are two separate processes taking place. The first is a transient process that occurs during movement initiation where, regardless of the curvature, a high lag between the movement and the neural representation of movement exists. The second consists of shorter lags correlated with movement curvature.

NEURAL IMAGE. An image of the trajectory represented by the population vectors can be formed by adding the vectors tip-to-

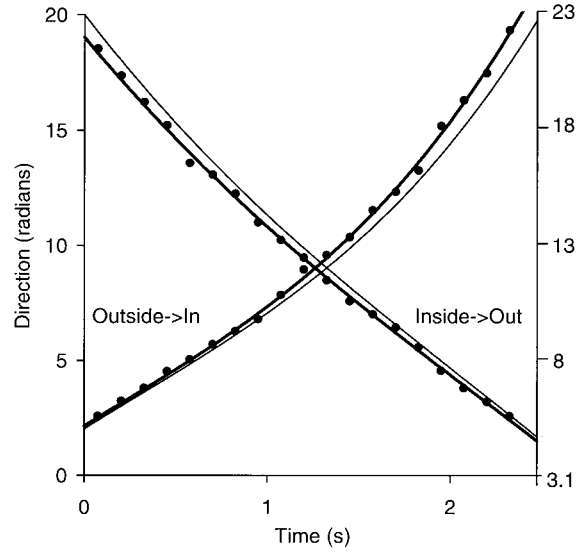

FIG. 7. Directional comparison between the movement (thin line) and population (thick line) vectors for both an outside→in (left ordinate) and inside→out (right ordinate) spiral. In both cases, the interior of the spiral is represented by high directional values (20–23 radians), whereas the outside of the spiral corresponds to small directions (2–5 radians). The same curvilinear relation of direction to time is present in both the population and movement vectors for both classes. The neural and movement directions are coincident in the outer portion of the spiral, but the neural directions lead those of the movement more as when the finger is moving in the inner portion of the spiral. The population directions (●), before smoothing and polynomial fitting, of every 5th population vector are shown to illustrate the nature of the raw data.

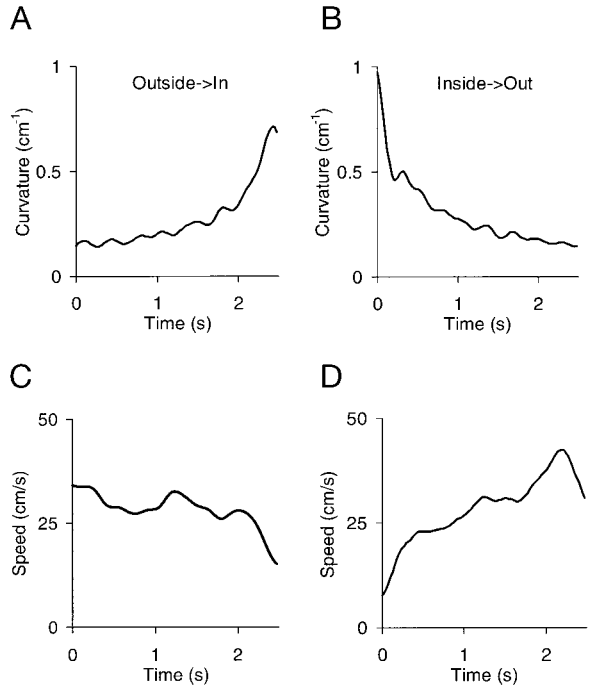

FIG. 8. Curvature and speed as a function of time for both classes of spirals. Curvature was low on the outside of the spiral and increased as the finger moved to the interior of the spiral (*A* and *B*). Although the finger speed profile was not consistent between the 2 classes, there was a tendency for finger speed to be high on the outside of the spiral and low in the interior (*C* and *D*) showing the inverse relationship between speed and curvature.

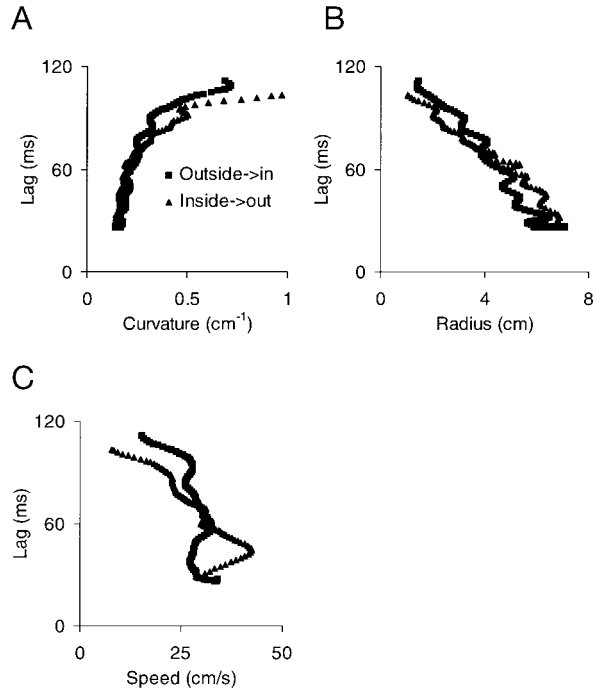

FIG. 9. *A*: comparison of curvature to prediction intervals. During low curvature drawing there appears to be only about a 30-ms lag between motor cortical activity and arm movement. This lag rapidly increases with curvature until reaching an asymptotic value of ~100 ms. *B*: same data as *A* with abscissa inverted showing a strong, consistent relation between the prediction intervals and radius of curvature. *C*: although not as consistent as curvature, an inverse relationship between finger speed and direction lag can be seen in the 2 classes of spirals.

tail. These neural trajectories are shown in Fig. 11. As expected with the high correlations between the movement and population vectors, the neural trajectories match closely the figures drawn with the finger. Due to the variable lags illustrated in Fig. 9, the highest fidelity outside→in spiral encompassed 97 bins of data (population vectors from 1 prebin and 96 task bins). On the other hand, the best matching inside→out spiral spanned 103 bins of data (4 prebins and 99 task bins). At the beginning of the outside→in task, the PI was small (~30 ms or 1 bin) and at the end of the movement, the PI was ~100 ms (4 bins). The prediction began only 1 bin ahead but ended 4 bins before the end of the actual movement for a total of 97 bins. In contrast, more bins are needed in the inside→out task, which started with a PI of 100 ms (~4 bins) and ended with a small PI of 30 ms (1 bin) for a net addition of three bins more than the movement.

COMPARISON OF PREMOTOR AND PRIMARY MOTOR CORTICAL POPULATION RESPONSE. The response of the premotor and primary motor cortical populations differ when compared with the vector algorithm. Our sample of premotor cortical cells was relatively small ($n = 77$) and because a few cells with responses not consistent with directional tuning can skew the population vector with small sample sizes (Georgopoulos et al. 1986), we applied an additional selection criterion to the premotor-primary motor cortical analysis. Only those cells that had at least 10% of their discharge rate during the spiral task explained by the directional tuning function ($r > 0.3$) were selected for this analysis. This resulted in a population of 50 premotor cells. A population of 50 primary motor cortical units ($r > 0.3$) from the same animal was compared with the same sized population of premotor cortical cells. A vectogram consisting of population responses from the two cortical areas is shown in Fig. 12. The motor cortical population still yields vectors that change directions smoothly through the movement. These are comparable to those in Fig. 6, which were

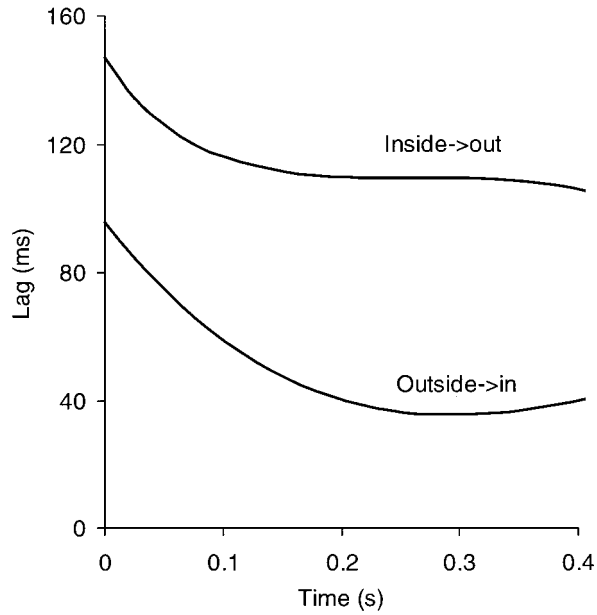

FIG. 10. Transient lags occurring during movement onset. During the movement initiation portion of the tracing task, both the outside→in and inside→out spiral have higher lags than would be expected during "steady-state" tracing. From 225 ms on, both spirals have lags matching those predicted by Fig. 9.

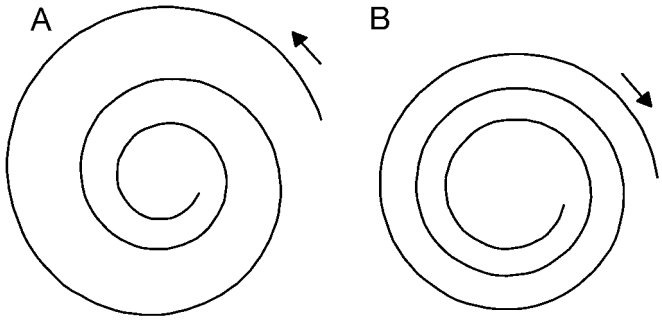

FIG. 11. Population trajectories for both an outside→in (*A*) and an inside→out (*B*) spiral movement. The trajectories were constructed by adding the individual vectors of Fig. 6 tip-to-tail (integrating).

composed of cells from three hemispheres. Vector correlations between the primary motor population vectors and the movement vectors yielded coefficients of 0.94 and 0.90 for the outside→in and inside→out spirals, respectively. In contrast, the premotor vectors change direction erratically yielding movement correlations of 0.62 (outside→in) and 0.82 (inside→out). This is evident in the neural trajectories derived from the vectors. In Fig. 13, *A* and *B*, the neural trajectories derived from primary motor data still show representations recognizable as spirals. However, the premotor neural trajectories in Fig. 13, *C* and *D*, have little resemblance to the drawn figure.

The horizontal speed components of the premotor neural and finger trajectories for the inside→out spiral were compared to help elucidate the distortion in the premotor neural trajectories. As shown in Fig. 14, there are two local peaks in the "neural" speed profile for every movement peak. One peak corresponds to the finger speed extremum; the other precedes it by an average of 250 ms. This, along with the timing of the individual neural responses of the premotor cortical cells shown in Fig. 5*B*, suggests that this population of premotor cortical cells is composed of two subpopulations, each of which generates trajectory signals that differ by ~250 ms. The timing of the

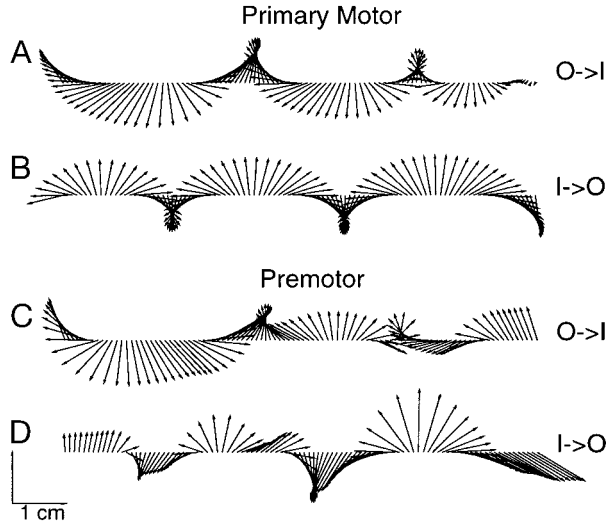

FIG. 12. Vectograms of population vectors generated from both primary (*A* and *B*) and premotor (*C* and *D*) cortical cells for both spiral tasks (*A* and *C*, outside→in; *B* and *D*, inside→out). The 100 vectors were generated from 50 cells in each cortical area of a single monkey during the spiral. With an equal number of cortical cells, the primary motor area contains a more consistent representation of the movement than does the premotor area.

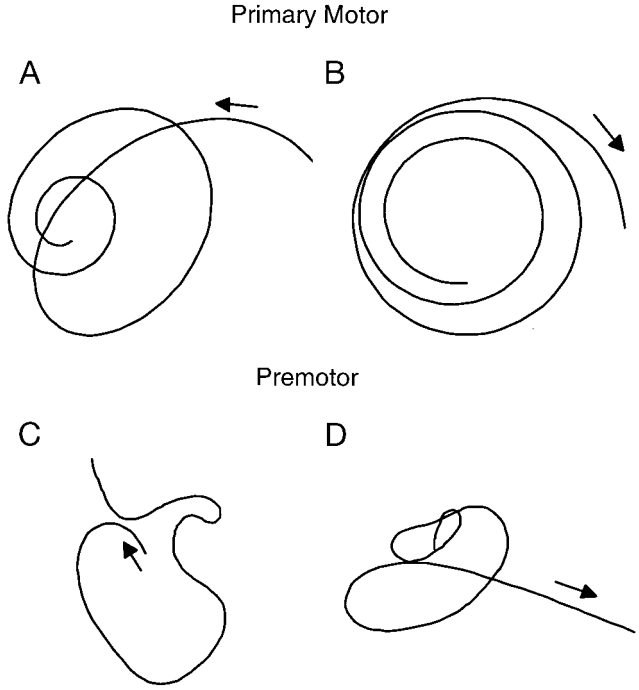

FIG. 13. Motor cortical population trajectories generated from the vectograms of Fig. 12. The outside→in class is on the *right* (*A* and *C*) and the inside→out is the *left column* (*B* and *D*). The finger trajectory is well represented, even in this small population of motor cortical cells (*A* and *B*). This is not true of the premotor cortical population (*C* and *D*).

premotor responses shown in Fig. 5*B* were used to separate the premotor cells into two groups. The activity patterns of those cells with an average lag >125 ms were shifted back in time by 250 ms. The data of cells with lags <125 ms were not shifted. The resulting neural trajectories are shown in Fig. 15. The distortions found in Fig. 13, *C* and *D*, are absent, showing that

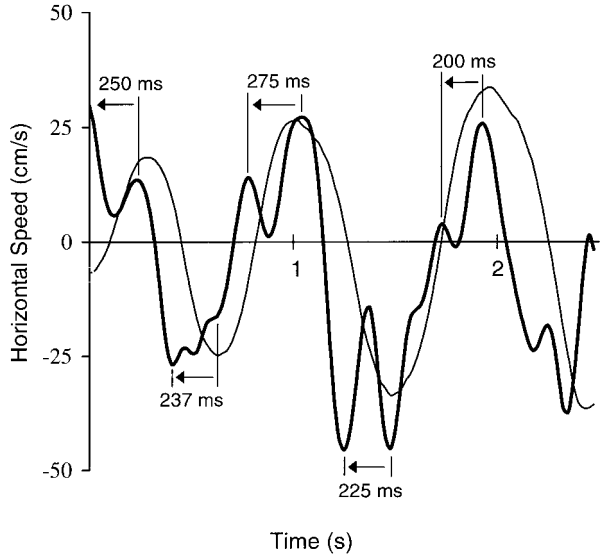

FIG. 14. Horizontal component of movement speed compared with that of the premotor population vector magnitude during an inside→out spiral. The premotor population magnitude (thick line) shows 2 local peaks for every movement peak (thin line), suggesting that the premotor area consists of 2 sets of cells coding for the same movement but at different points in time. One set of cells matches the movement ~250 ms beforehand, whereas the 2nd set is synchronous with the movement.

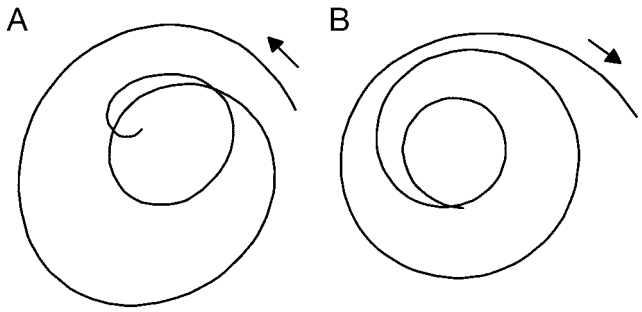

FIG. 15. Lag-adjusted premotor population trajectories. All cells having an average interval >125 ms had their firing rates shifted back in time by 250 ms. Those having average intervals <125 ms were not altered. A new set of population vectors was constructed yielding a better match to the movement (*A*: outside→in, *B*: inside→out).

they were due to timing differences between the two subpopulations of cells in the premotor cortex. The locations of the cells in the two subpopulations were analyzed to determine whether they came from distinct regions or layers within the dorsal premotor area, but there was no anatomic distinction.

Joint angles and angular velocity

Joint angle information was collected for the right arm of *subject 2*. A total of 465 individual trials were recorded and averaged. In Fig. 16, 4 DOF about the shoulder and elbow joints are plotted for both tracing directions. To demonstrate superimposition, the inside→out data were plotted in reverse order from that of the outside→in task. The data were superimposed and showed that the monkey had approximately the same instantaneous arm posture for both tracing directions.

Arm posture and finger position were well correlated in these tasks. Because instantaneous arm posture determines finger position, the angular velocities of the joints are correlated with hand velocity. This raises several possibilities; for instance, the latency between cortical signal and shoulder/elbow displacement could be fixed so that the curvature-related prediction intervals in the population analysis resulted from a variable phase between finger velocity and joint angular velocities of the proximal arm. Another possibility is that finger and joint displacements were phase locked; then the variable lag would lie between cortex and all kinematic variables. To address this issue, the relative phases between the directional component of finger velocity and the four joint angular velocities were analyzed. The first maximum in a joint angular velocity for the outside→in task was used to determine an offset or bias term for the joint angular velocity. This allowed the finger velocity and a joint angular velocity to be initially aligned so it would be easier to observe any variations in phase. By plotting joint angular velocity and the cosine of finger direction $\cos(\theta - \theta_{bias})$, the change in phase between these two variables can be assessed.

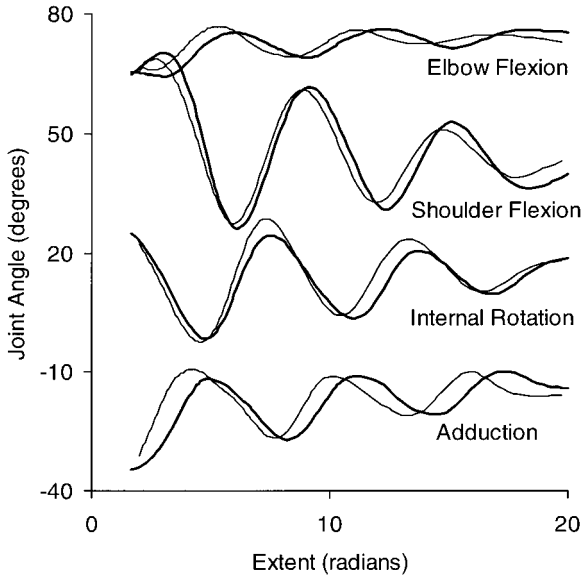

FIG. 16. Joint angles as a function of extent (position on the spiral) for both classes of spirals. Elbow flexion, shoulder flexion, internal rotation, and adduction were generated from direction cosines (Cardanic form) of upper and forearm attitudes. The high degree of overlap between the 2 classes suggests that instantaneous arm postures for a given location on the spiral were similar between the 2 tasks. Because movement direction and single-cell activity also varied harmonically throughout the task, joint angular velocity would be expected to covary with these parameters as well. The anatomic position represents all joint angles being zero.

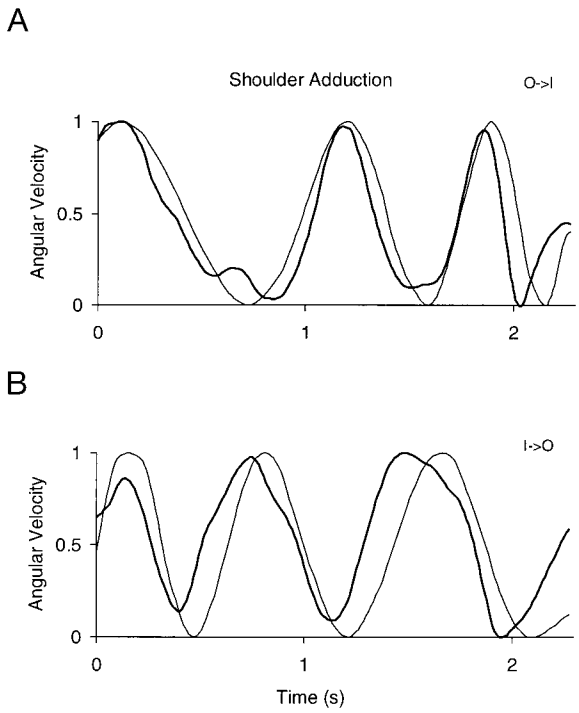

FIG. 17. Phase relation between a proximal arm intrinsic coordinate (shoulder adduction velocity) and a distal arm extrinsic coordinate (finger velocity). Shoulder adduction velocity (thick line) is plotted against cosine of finger direction. In both classes the phase lag is initially zero but increases (*A*: outside→in lag = 25 ms; *B*: inside→out lag = 150 ms) as the task progresses regardless of curvature, suggesting that the variable cortical lags shown in Fig. 7 are not simply due to phase lag in proximal-to-distal arm kinematics.

Three of the four joint angles measured in this study were found to have a constant phase relationship with finger velocity. Shoulder adduction, the only joint angular velocity found to have a significant variable phase relationship, is shown in Fig. 17. During the outside→in task, the phase between these components is initially zero with a slight phase advance (~25 ms) occurring at the end of the movement. Although shorter than the 75-ms change in prediction interval found for the cortical responses, this small phase advance is consistent with the hypothesis that the variable prediction interval could be a

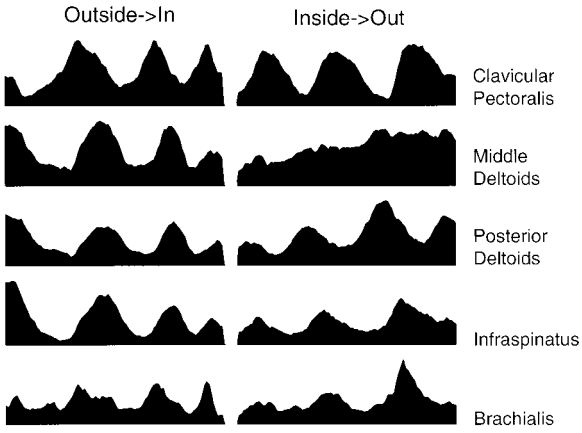

FIG. 18. Average EMG activity for the left arm of Subject 1 for both classes of spirals. Each histogram is generated from 75 trials recorded over multiple days using epimysial electrodes. The left column corresponds to the outside→in class and the right to the inside→out class. With the exception of middle *deltoids* in the inside→out class, all the muscles show harmonic activity similar to cortical activity.

property of proximal-to-distal kinematic lags. However, the possibility that the shoulder component is directly linked to cortical activity is eliminated in the inside→out task because the phase between the two velocity components increases by >150 ms during the outward progression of the hand. This phase relation is opposite to the decreasing prediction interval between cortical activity and hand velocity. Hence none of the joint angles had a constant phase relationship with cortical activity.

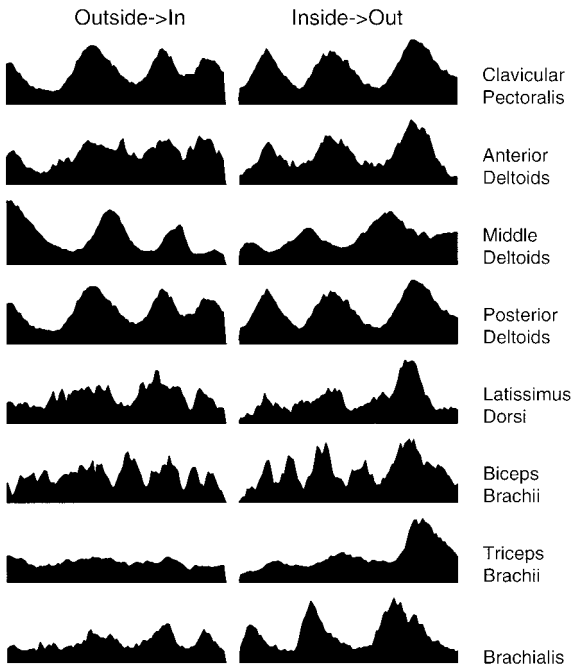

FIG. 19. Average EMG activity for the left arm of *subject 2* for both classes of spirals. Like Fig. 18, EMG data were combined over multiple days. Intramuscular fine wire electrodes, inserted daily, were used to collect the data. The *left column* corresponds to the outside→in class and the *right* to the inside→out class. With the exception of *biceps brachii*, all the muscles showed the same stereotypic response seen in Fig. 18. *Biceps brachii* has approximately twice as many peaks in EMG as the other muscles.

EMG response

The muscular activity in the left arms of both monkeys was recorded in a subset of the total trials. *Subject 1* had chronic epimysial electrodes implanted on *clavicular pectoralis, middle deltoids, posterior deltoids, infraspinatus,* and *brachialis* muscles. A total of 75 individual trials were recorded for both the outside→in and inside→out classes. Figure 18 shows the average activity in each of these muscles over all recorded trials. Similarly, intramuscular activity was recorded from eight muscles of *subject 2*. The average EMG activity recorded in *clavicular pectoralis* ($n = 95$ experiments), *anterior deltoids* ($n = 35$), *middle deltoids* ($n = 165$), *posterior deltoids* ($n = 170$), *latissimus dorsi* ($n = 40$), *biceps brachii* ($n = 15$), *triceps brachii* ($n = 145$), and *brachialis* ($n = 50$) can be seen in Fig. 19. With the exception of *biceps brachii*, all of the muscles recorded have responses that are temporally similar to both movement direction and cortical activity. Because EMG activity covaries well with movement direction, the variable lags seen in the population response could be due to earlier activation of muscles during higher curvature. With the use of the EMG's preferred direction information calculated from center→out task, a predicted versus actual EMG activity plot was made. Because the predicted EMG activity is generated from finger kinematics, the plots essentially compare EMG activity with finger velocity. However, the muscle activities behaved the same way as the angular velocities of the joints. They either remained phase locked to the finger or like the shoulder adductor infraspinatus (Fig. 20), the finger lagged the muscle more later in the task.

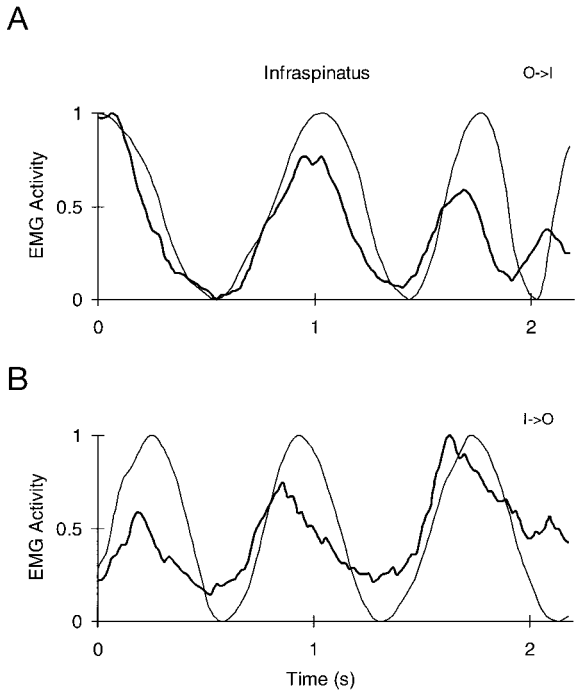

FIG. 20. Simulated and actual EMG activity for infraspinatus muscle of *subject 1*. The simulated EMG was generated from the center→out tuning parameters of the muscle and finger velocity during spiral tracing. The actual EMG activity (thick line) preceded and matched well the simulated activity (thin line) by 75 ms on average. The phase relationship between the peaks in activity was found to be similar to the joint angular velocities (Fig. 17). In the outside→in case (*A*) the lag between the 2 representations was ~0 and increased to 75 ms at the end of the movement. In the inside→out case (*B*) the lag started out ~50 ms and increased to 100 ms.

DISCUSSION

The population vector algorithm shows that hand trajectory is well represented in the activity of motor cortical cells (Georgopoulos et al. 1988; Moran and Schwartz 1999; Schwartz 1993, 1994; Schwartz and Moran 1999). In this study we show not only that the spatial attributes of a complex movement are encoded in this activity, but that the timing of this isomorphic representation relative to the movement changes in a characteristic way that is determined by the shape of the figure. As a tool, the population vector algorithm has proven to be useful in showing that movement direction is an important parameter encoded in many brain areas (Caminiti et al. 1990; Fortier et al. 1989; Georgopoulos et al. 1984; Kalaska et al. 1983; Motter et al. 1987; Ruiz et al. 1995; Snowden et al. 1992). Furthermore, this algorithm has shown how populations of cells encode parameters that single cells cannot. In this model, we make a tacit assumption that contributions from individual cells are being summed at the same node to form a population vector. Although the model succeeds as a predictor of movement kinematics, there is no convincing evidence of such a node. Even when the movement itself is considered as the convergence point, our results show that the signals reaching it traversed pathways of different durations as the task progressed.

The spiral drawn in this task consisted of three concentric circuits with smoothly changing radii. Many movement parameters change in a cyclic manner when this type of figure is drawn. Finger direction and many of the joint angles changed harmonically during this task as did single-cell and EMG activity. Within a given task, the correlation of these parameters to each other makes it difficult to distinguish the effect of cortical activity in generating these modulated patterns. However, several points can be addressed by considering timing and movements in both directions. The timing between the instantaneous directional signal in the cortical population and finger direction varies throughout each drawing task. This prediction interval is position dependent; it is large where curvature is high and smaller on the outside of the spiral regardless of drawing direction. Although the prediction interval may be determined by the figural aspects of the task, the neuronal activity at a given location along the spiral is very dependent on the direction of movement.

One possibility for variable lags is intersegment delays along the arm. Variable lags were found between shoulder adduction and finger movement. However, the variable lags were not position dependent. For both tracing directions, the intersegment delays were low during the initial part of the movement and increased as the movement progressed. Another possible contribution to the observed lags may be the delays between muscle activation and limb displacement. However, a comparison of EMG modulation and hand direction showed the same pattern as that of the joint angles, suggesting that proximal-arm muscle activity and proximal-arm kinematics are phase locked. It is unlikely that the variable lags found in this task can be better reconciled with an intrinsic coordinate system. However, other reference frames, such as the affine coordinate system initially used in vision research and more recently in motor control (Pollick and Sapiro 1997), may provide a constant lag relationship with cortical activity, suggesting that movements may be planned in a non-Euclidean reference frame.

Another possibility is that the time-varying lags between cortical activity and finger velocity could be explained by higher order terms (e.g., acceleration), accounting for a higher percentage of cortical discharge during higher curvatures. In the spiral tasks, as the curvature increases, the tangential velocity decreases, whereas at the same time both normal and tangential accelerations increase. Because normal acceleration is always directed toward the center of the spiral, it is position dependent. For the inside→out spiral, the normal acceleration will lead the tangential velocity by 90°, but for the outside→in spiral, it will lag tangential velocity by 90°. If the normal acceleration did alter the lags, it would cause an increased phase lag for higher curvatures in the outside→in spiral but a decreased phase lag for higher curvatures for the inside→out spiral, which is inconsistent with the observed prediction intervals.

Unlike normal acceleration, tangential acceleration always leads tangential velocity by 90° *phase* shift. If it is assumed that the activity of a motor cortical cell were modulated by both tangential velocity and tangential acceleration, then the phase lag (measured in degrees) would increase under higher curvatures. However, because the cycle time or period decreases in the inner portion of the spiral, the *time* lag (measured in ms) between tangential velocity and tangential acceleration decreases. Assuming the worse case scenario (i.e., cortical activity is composed of 50% velocity coding and 50% acceleration coding), the net affect of the increased tangential acceleration and decreased tangential velocity in high curvature areas would actually slightly reduce the time lag, making it unlikely that acceleration (normal or tangential) contributes to the observed time lags between cortical activity and movement.

The curvature-dependent lags differ from those observed at movement initiation and suggests that the process of movement initiation is distinct from that underlying intramovement control. At the beginning of both tasks, there is a curvature-independent, transient lag of ~150 ms, similar to that found in point-to-point movements. This initiation process subsides ~225 ms after the finger left the start target, after which the lags become curvature dependent. The initial portion of a reach is somewhat ballistic, and there may be a similar lack of feedback control at the beginning of the drawing task. The subsequent variable lags may be indicative of visual feedback that becomes important in the ongoing tracing. A similar finding was made in the oculomotor saccade control system (Munoz et al. 1991). At the beginning of a saccade, superior colliculus output neurons fire at least 25 ms ahead of movement initiation, whereas within a saccade their activation results in an acceleration change within 10 ms.

The changes in PI were directly related to the instantaneous radius of the figure. During straight drawing, the population vector directions match that of the trajectory, and it is unlikely that the signal is functioning in a predictive or causal manner because the PI is small. Although both direction and speed are always represented accurately, when the PI is small, the output of the motor cortex may reflect corollary discharge generated in synchrony with the movement. For straight paths, a "keep moving in the same direction" signal transmitted once would be more efficient than continuous transmission of the same direction. The timing lag between cortical signal and movement may be related to the amount of intervening processing required to generate the movement represented centrally by the

population vector. For regions of higher curvature, the motor cortical PI is large, and the signal represented in this portion of the neural trajectory may contribute to the underlying mechanism of trajectory generation. Studies examining the representation of different movement parameters (Ashe and Georgopoulos 1994; Fu et al. 1995; Kalaska et al. 1989; Schwartz 1992) find that direction is the predominant parameter represented in the discharge of motor cortical cells. If the motor cortex can be considered an important structure for the processing of movement direction, it would be reasonable that within a continuous movement, this function comes into play only when direction changes rapidly, in regions where the path is curved. In this interpretation, more processing is required when direction changes rapidly over a short distance.

Timing considerations also have the potential to elucidate processing between different neural structures. Our results show that premotor cortical cells seem to be divided into two populations: those that encode the direction synchronously during drawing and those that predict it by ~250 ms. Because the PI in the primary motor cortex is midway between the intervals of these two subpopulations and there is a well-established reciprocal linkage between these cortical areas, these results might be interpreted as evidence for a functional loop. However, it is difficult to account for the long latency (125 ms) between the appearance of corresponding direction signals in the different populations. Even an indirect path through subcortical structures would have a characteristic loop time that was much shorter than this.

There are other possible explanations for these results. In a circular task such as spiral drawing, the variables of interest typically have harmonic (i.e., sinusoidal) components. The derivative of a sinusoidal signal is another sinusoidal signal shifted by 90°. The 250 ms seen between the two subpopulations of premotor cells corresponds to a 90° phase shift in the spiral task (each circuit takes ~1 s). Thus the subpopulation with a 250-ms direction lag could actually be an acceleration signal and the later premotor subpopulation a velocity representation.

The demonstration of an isomorphic representation of endpoint trajectory in these cortical cells makes it possible to study the instantaneous latencies between this representation and movement. There are a number of explanations for the elastic nature of this latency. Some of these are related to mechanics—time delays through a series of joint rotations, and muscle excitation-displacement lags are examples of these. Our data suggest that the timing relations of these factors cannot account for the variable lags in both directions of tracing. However, there are complex phase relations between many peripheral motor elements that may contribute to these elastic lags. Directional comparison of EMG activity and hand trajectory shows that the muscle activity occasionally leads arm displacement by magnitudes as large as those between neural activity and movement, suggesting a complex relation between cortical output, muscle contraction, and arm displacement. However, the clear, consistent relation between prediction interval and curvature and the robust representation of trajectory in these motor cortical areas suggests that direction-related parameters such as curvature (change in direction/distance) and angular velocity (change in direction/time) are important in determining the way that the output of these areas eventually contributes to the generation of movement.

A. Kakavand trained the animals and assisted in the experiments.

This work was supported by the Neurosciences Research Foundation, the Barrow Neurological Institute, and National Institute of Neurological Disorders and Stroke Grant NS-26375.

Address for reprint requests: A. B. Schwartz, The Neurosciences Institute, 10640 John Jay Hopkins Dr., San Diego, CA 92121.

Received 8 December 1997; accepted in final form 21 August 1998.

REFERENCES

ASHE, J. AND GEORGOPOULOS, A. P. Movement parameters and neural activity in motor cortex and area 5. *Cereb. Cortex* 6: 590–600, 1994.

CAMINITI, R., JOHNSON, P. B., BURNOD, Y., GALLI, C., AND FERRAINA, S. Shift of preferred directions of premotor cortical cells with arm movements performed across the workspace. *Exp. Brain Res.* 83: 228–232, 1990.

FORTIER, P. A., KALASKA, J. F., AND SMITH, A. M. Cerebellar neuronal activity related to whole-arm reaching movements in the monkey. *J. Neurophysiol.* 62: 198–211, 1989.

FU, Q.-G., FLAMENT, D., COLTZ, J. D., AND EBNER, T. J. Temporal encoding of movement kinematics in the discharge of primate primary motor and premotor neurons. *J. Neurophysiol.* 73: 836–854, 1995.

GEORGOPOULOS, A. P., KALASKA, J. F., CRUTCHER, M. D., CAMINITI, R., AND MASSEY, J. T. The representation of movement direction in the motor cortex: single cell and population studies. In: *Dynamic Aspects of Neocortical Function*, edited by G. M. Edelman, W. E. Goll, and W. M. Cowan. New York: Wiley, 1984, p. 501–524.

GEORGOPOULOS, A. P., KETTNER, R. E., AND SCHWARTZ, A. B. Primate motor cortex and free arm movements to visual targets in three-dimensional space. II. Coding of the direction of movement by a neuronal population. *J. Neurosci.* 8: 2928–2937, 1988.

GEORGOPOULOS, A. P., SCHWARTZ, A. B., AND KETTNER, R. E. Neuronal population coding of movement direction. *Science* 233: 1416–1419, 1986.

KALASKA, J. F., CAMINITI, R., AND GEORGOPOULOS, A. P. Cortical mechanisms related to the direction of two-dimensional arm movements: relations in parietal area 5 and comparison with motor cortex. *Exp. Brain Res.* 51: 247–260, 1983.

KALASKA, J. F., COHEN, D.A.D., HYDE, M. L., AND PRUD'HOMME, M. A comparison of movement direction-related versus load direction-related activity in primate motor cortex, using a two-dimensional reaching task. *J. Neurosci.* 9: 2080–2102, 1989.

LACQUANITI, F., TERZUOLO, C., AND VIVIANI, P. The law relating kinematic and figural aspects of drawing movements. *Acta Psychol.* 54: 115–130, 1983.

MORAN, D. W. AND SCHWARTZ, A. B. Motor cortical representation of speed and direction during reaching. *J. Neurophysiol.* 82: 000–000, 1999.

MOTTER, B. C., STEINMETZ, M. A., DUFFY, C. J., AND MOUNTCASTLE, V. B. Functional properties of parietal visual neurons: mechanisms of directionality along a single axis. *J. Neurosci.* 7: 154–176, 1987.

MUNOZ, D. P., GUITTON, D., AND PELISSON, D. Control of orienting gaze shifts by the tectoreticulospinal system in the head-free cat. *J. Neurophysiol.* 66: 1642–1666, 1991.

POLLICK, F. E. AND SAPIRO, G. Constant affine velocity predicts the 1/3 power law of planar motion perception and generation. *Vision Res.* 37: 347–353, 1997.

RICHMOND, B. J., OPTICAN, L. M., PODELL, M., AND SPITZER, H. Temporal encoding of two-dimensional patterns by single units in primate inferior temporal cortex. I. Response characteristics. *J. Neurophysiol.* 57: 132–146, 1987.

RUIZ, S., CRESPO, P., AND ROMO, R. Representation of moving tactile stimuli in the somatic sensory cortex of awake monkeys. *J. Neurophysiol.* 73: 525–537, 1995.

SCHWARTZ, A. B. Motor cortical activity during drawing movements. Single-unit activity during sinusoid tracing. *J. Neurophysiol.* 68: 528–541, 1992.

SCHWARTZ, A. B. Motor cortical activity during drawing movements: population response during sinusoid tracing. *J. Neurophysiol.* 70: 28–36, 1993.

SCHWARTZ, A. B. Direct cortical representation of drawing. *Science* 265: 540–542, 1994.

SCHWARTZ, A. B. AND MORAN, D. W. Motor cortical activity during drawing movements: population representation during lemniscate tracing. *J. Neurophysiol.* 82: 2705–2718, 1999.

SHADMEHR, R. AND MUSSA-IVALDI, F. A. Adaptive representation of dynamics during learning of a motor task. *J. Neurosci.* 14: 3208–3224, 1994.

SNOWDEN, R. J., TREUE, S., AND ANDERSEN, R. A. The response of neurons in areas V1 and MT of the alert rhesus monkey to moving random dot patterns. *Exp. Brain Res.* 88: 389–400, 1992.

WOLTRING, H. J. A FORTRAN package for generalized, cross-validatory spline smoothing and differentiation. *Adv. Eng. Software* 8: 104–113, 1986.